REVISTA IBRACON DE ESTRUTURAS E MATERIAIS
IBRACON STRUCTURES AND MATERIALS JOURNAL

Computational modeling of steel fiber reinforced concrete beams subjected to shear

Modelagem computacional de vigas de concreto armado reforçado com fibras de aço submetidas a cisalhamento

D. L. ARAÚJO [a]
dlaraujo@eec.ufg.br

L. C. CARMO [b]
luccarmo@gmail.com

F. G. T. NUNES [c]
fgtiburcio@gmail.com

R. D. TOLEDO FILHO [d]
toledo@coc.ufrj.br,

Abstract

Computational modeling has become a common activity to Civil Engineering researchers and professionals. Therefore, the knowledge about the mechanical behavior of materials is very important. To correctly model the mechanical behavior of concrete structures subjected to shear stress, it is necessary to determine the shear retention factor that accounts for the friction between the two surfaces of a crack. The objective of this study is to show how the shear retention factor of steel fiber reinforced concrete can be obtained from direct shear tests associated to computational modeling. A concrete matrix with compressive strength of 60 MPa, to which 1% and 2% content of steel fibers were added, was used for the shear tests. The stress-slip relationship was obtained from these tests, and the shear retention factor of the steel fiber reinforced concrete was determined from inverse analysis using the Finite Element Method software DIANA© 8.1.2. Finally, the shear retention factor and the influence of steel fibers on the cracks were validated from the computational modeling of steel fiber reinforced concrete beams subjected to shear available in the literature.

Keywords: *Shear, Steel Fiber Reinforced Concrete, Computational Modeling.*

Resumo

A modelagem computacional cada vez mais se torna parte integrante das atividades dos pesquisadores e profissionais da área de engenharia civil. Para isso, o conhecimento do comportamento mecânico dos materiais é de fundamental importância. No caso das estruturas de concreto submetidas a esforços de cisalhamento, para a correta representação do seu comportamento é necessária a determinação do fator de retenção do cisalhamento. Neste trabalho, procura-se determinar esse fator para concretos reforçados com fibras de aço por meio de ensaios de cisalhamento direto em corpos-de-prova prismáticos associados à modelagem computacional. Foi estudada, em laboratório, uma matriz de concreto com resistência à compressão de 50 MPa, à qual foram adicionadas 1,0% e 2,0% de fibras de aço. A relação tensão *versus* deslizamento foi determinada experimentalmente, sendo em seguida realizada uma análise inversa dos corpos-de-prova de modo a se determinar o fator de retenção do cisalhamento do concreto reforçado com fibras de aço. Para tanto, foi utilizado o programa comercial de elementos finitos DIANA© 8.1.2. Ao final, o fator de retenção do cisalhamento, bem como a influência das fibras na fissuração, foi validado por meio da modelagem de vigas de concreto armado reforçado com fibras de aço submetidas a esforços de cisalhamento disponíveis na literatura.

Palavras-chave: *Cisalhamento, Concreto Reforçado com Fibras de Aço, Modelagem computacional.*

[a] *Associate Professor, Pos-Graduate Program in Geotechnical Engineering and Civil Construction - School of Civil Engineering – Federal University of Goiás, dlaraujo@eec.ufg.br, Praça Universitária, s/n, Setor Universitário, 74605-220, Goiânia, GO;*

[b] *M.Sc. Degree, School of Civil Engineering – Federal University of Goiás, luccarmo@gmail.com, Praça Universitária, s/n, Setor Universitário, 74605-220, Goiânia, GO;*

[c] *M.Sc. Degree, School of Civil Engineering – Federal University of Goiás, fgtiburcio@gmail.com, Praça Universitária, s/n, Setor Universitário, 74605-220, Goiânia, GO;*

[d] *Associate Professor, COPPE/UFRJ, toledo@coc.ufrj.br, Caixa Postal 21945-970, Rio de Janeiro, RJ.*

1. Introduction

The use of software has become essential for engineers and researchers who develop formulations and numerical codes that simulate the behavior of structures in order to obtain parameters that ensure economy, safety, and agility of structural designs.

The numerical analysis of reinforced concrete is particularly complex. Being a composite material, the reinforced concrete has characteristics that make difficult the reproduction in a computational environment all variables present in a service life of the structures, such as multiple cracks and reinforcement slip. Hence, approximations are used and most of the times they fulfill structural project needs (safety and economy).

Specifically, regarding the numerical study of the shear stress on the reinforced concrete structures, there is a number of theoretical and experimental studies on concrete beam subjected to shear [1-3] although numerical studies on this subject are not so common. Most of the studies about computational modeling of concrete structures deals with flexion problems [4], and numerical models to shear available do not detail stress and strain distributions along the structure, nor do they provide details on the cracking patterns. The numerical models available for the treatment of concrete structures are based on the Finite Element Method (FEM) [5]. On FEM models, the cracking analysis can be classified as smeared crack model or discrete crack model.

The discrete crack model is the most refined model, and it is more adequate when there is a small number of cracks in the structure. Nevertheless, the difficulty in using such model lies on locating the crack propagation route and the need of reorganizing the continuous mesh as they progress. The most commonly used model is the cohesive crack model developed by Hillerborg [6] for mode I fracture of quasi-brittle materials (such as concrete), which was later adapted to the mixed-mode fracture (modes I and II) [7].

In the smeared crack model, pioneer in the crack analysis [8], a great number of parallel cracks, which present theoretically tiny openings, are smeared over the finite-element mesh that modeling the continuous media, which does not change with the crack propagation. This propagation is simulated with the softening of the continuous media material; hence the cracks can be fixed (defined orientation angle) or rotated (variable orientation angle). Researchers state that the model with rotated cracks tends to be more stable than the model with fixed cracks [9]. The smeared crack model is the most common due to the simplicity of cracks. However, it presents some solution convergence problems, so some mathematical adjustments of the constitutive models are necessary. Since the method does not consider the cracks discrete entities, it prevents the direct determination of the crack tip opening (dimension perpendicular to the propagation direction).

Using the commercial finite element software DIANA© 8.1.2 [10], this paper shows a numerical study on the steel fiber reinforced concrete subjected to shear adopting the smeared crack model. The software DIANA© allows a consideration of embedded steel reinforcement in the continuous, therefore, the reinforcement in concrete beams can be analyzed as finite element of bars enabling the determination of stress and strain on them. To represent the shear stress transfer across the cracks, the shear retention factor is applied, and its value is obtained from inverse analysis of the direct shear tests.

2. Models to computational modeling of concrete subjected to shear

This section presents briefly some of the numerical models used for the computational modeling of concrete using the commercial software DIANA© 8.1.2 [10], which is based on the finite element method for the analysis of several different structures. The concrete constitutive models include cracking effects and embedded steel reinforcement, or a combination of them. Moreover, the software allows the analysis of other complex phenomena such as creep, curing, temperature, and instability.

The software includes two models for modeling the structural behavior of the cracked concrete: smeared crack model and the discrete crack model. Concepts of the fracture mechanics are introduced, so that the results become independent of the mesh used. The main parameters related to the fracture mechanics introduced in the smeared crack model are the fracture energy (G_f^I), the compressive fracture energy (G_c) and crack bandwidth. Besides, the software DIANA© allows the use of the CEB-FIP Model Code 1990 [11] and of curves defined by the user. The crack bandwidth (h_{cr}) should correspond to a representative dimension of the mesh elements, and it depends on the shape and kind of the element.

The smeared crack model determines the crack tip opening and orientation in a specific region using "Incremental Plastic Models" and "Total Strain Crack Models". The Total Strain models describe the tensile and compressive behavior of a material with one stress–strain relationship. Thus, it is very well suited for analyses which are predominantly governed by cracking or crushing of the material and it is represented by the Rotating Crack Model and by the Fixed Crack Model. In the formulation of the Incremental Plastic Models, the concepts of the theory of plasticity are used classifying the strains as elastic (reversible) and plastic (irreversible). The Multi-Directional Crack Model, which represents this formulation in the DIANA© software, presents advantages for modeling bi-dimensional problems [10].

It is natural to consider that the material shear rigidity reduces due to cracking, which is represented by the shear retention factor. The DIANA© software offers three different relations to deal with this effect: full shear retention, constant shear retention, and variable shear retention. In the full shear retention, the elastic shear modulus (G) is not reduced, which implies that the secant crack shear stiffness is infinite. In case of reduced shear stiffness, the shear retention factor β is less or equal to one, but greater than zero. Considering the variable shear retention, the shear retention factor is a function of the crack tip opening [10].

The reinforcement of concrete structures can be modeled using an embedded reinforcement. Such elements enable the definition of discrete reinforcement (active or passive bars) and distributed reinforcement (or grid reinforcement) in bi-dimensional and tri-dimensional structures. With those elements, it is considered the perfect bond between the concrete and the reinforcement, i.e., there is no slip between them. For some analyses, the reinforcement can be modeled by truss elements and connect them to the surrounding concrete via structural interface elements. The interface elements can be modeling the bond-slip effect.

The crack tip opening is not determined in smeared crack models. Nevertheless, it can be estimated since the total strain includes an elastic strain and a crack strain due to the principal stress on Gauss points reaches the tensile strength of the concrete. If the interpolation func-

Table 1 – Mixture proportion of concrete (quantities per m³)	
Material	**Quantity**
Cement CP III-40-RS (kg)	440
Silica Fume (kg)	35
Natural Sand (kg)	817
Coarse Aggregate (kg)	817
Water (kg)	198
Wollastonite Micro-fibers (kg) *	72.5 (2.5%)
High-range water-reducing admixture (kg)**	5.86 (1.2%)
Ratio W/(Cement + Silica)	0.40
* Volumetric fraction; ** cement plus silica fume mass percentage	

Table 2 – Direct shear tests on prismatic specimens	
Specimen	**Fiber Volume Amount , V_f(%)**
CP-60-0-12.5	0,0
CP-60-1-12.5	1,0
CP-60-2-12.5	2,0

tion of the finite element used in the analysis is know, the strain field throughout the element can be determined. For a finite element with a linear interpolation function, the strain field throughout the element is constant. Therefore, the crack tip openings can be estimated by multiplying the strain at Gauss points by the distance between those points. If the shear crack inclination is 45°, which is plausible for beams without transverse reinforcement, the distance on the diagonal between the Gauss points (considering a rectangular finite element) can be taken. This procedure can be extrapolated; in such an event, the distance on the diagonal between the finite element nodes in question is taken.

3. Materials and Experimental Procedure

3.1 Materials

A concrete matrix with compressive strength values of 50 Mpa was developed on the 28th day. The mix proportions per cubic meter of concrete are given in table 1. Different amount of Dramix® RC 65/35 BN steel fibers (1.0% and 2% which is equivalent to 79 kg/m³ and 157 kg/m³, respectively) with tensile strength of 1150 MPa were added to the matrix. The steel fibers were hooked ends with length of 35 mm and aspect ratio of 65. The amount of 2.5%, in volume of concrete, of the Wollastonite micro-fibers was also added to the matrix. These micro-fibers work as the reinforcement required in the first steps of the matrix cracking. The cement used was CP III 40 RS and the fine aggregate was natural sand, with maximum size of 4.8 mm, and the coarse aggregate was 12.5 mm maximum size. The mixtures were produced in a planetary concrete mixer and the specimens were kept in a wet chamber until the conduction of the test.

The hardened concrete with and without fibers were characterized to compressive strength (f_{cm}), according to the Brazilian Standard NBR 5739 [12], and to tensile splitting strength ($f_{ctm,sp}$) according to Brazilian Standard NBR 7222 [13]. The tests were conducted in cylindrical specimens with 150 mm diameter and 300 mm height.

3.2 Direct shear test

The specimens used in these tests were 150 mm (width) x 150 mm (height) x 600 mm (long). The objective of this test was to determine the shear stress-slip relationship of the steel fiber reinforced concrete and thus verify the influence of the fibers on the shear strength and ductility of the concrete.

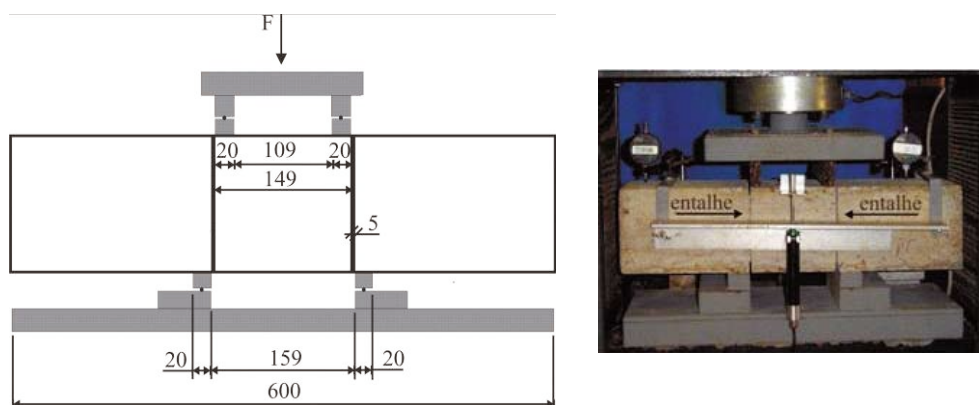Figure 1 – Scheme of direct shear test on prismatic specimen (dimensions in mm)

Figure 2 – Direct shear test equipment

distance of 149 mm from one external side to another. The specimen was placed on another rigid metallic block with two choppers of 20 mm thickness and 150 mm length and placed at a distance of 159 mm from one internal side to another.

The vertical displacement of the central region between the grooves was measured by a linear position transducer of maximum displacement length of 100 mm. Such displacement represents the average displacement of the two shear plans (figure 1). The tests were conducted under displacement control using a universal electromechanical testing machine of 1000 kN capacity (figure 2).

4.   Results

Table 3 shows the maximum load (F_{max}) and the maximum shear strength (τ_u) on the specimens. Those values were divided by two, i.e., by the number of shear plans. On average, the addition of 1% and 2% amount of fibers increased the shear strength in approximately 110% and 133%, respectively, when compared to the matrix. This table also shows the correlation constant, k, between the average shear stress and the concrete average compressive strength as follows.

$$\tau_u = k\sqrt{f_{cm}} \qquad (1)$$

Table 2 shows the nomenclature of specimens and the volume fraction of the fiber added. Identical specimens were made for the tests with fiber reinforced concrete, and four specimens were made for the tests without fibers.

The tests were based on previous studies reported in the literature [14]. The specimens were sawed at 15 mm along the perimeter of the transversal section in the region where a shear crack was expected. Hence, the dimension of the shear strength section was 120 mm x 120 mm (Figure 1).

In this test, the load was applied using a metallic block with two choppers of 20 mm thickness and 150 mm length and placed at a

There is an increase in the value of the constant k with the increase of the volume of the fibers and the concrete compressive strength. This is due to the increased volume of the fibers present in the mixture as well as to the increased compressive strength of the fiber reinforced concrete.

Figure 3 shows the load versus slip curves of the specimens. Analyzing the specimens without fibers, it can be seen a first peak load, which refers to the crack in the shear plan (matrix rupture), and a second peak load, which refers to the rupture of the specimen. This shear strength increase even after the shear crack is due to the aggregate interlock along the shear plan. The increase of strength due to the aggregate interlock in the tests showed dispersion for the four specimens (20%, 10%, 58% e 74%).

Table 3 – Maximum load and shear strength on a shear plan

Specimen	Specimen number	V_f (%)	f_{cm} (MPa)	F_{max} (kN)	τ_u (MPa)	k
CP-60-0-12.5	1	0.0	51.77	119.93	8.13	1.13
	2			85.53	5.79	
	3			122.96	8.33	
	4			152.06	10.39	
CP-60-1-12.5	1	1.0	65.27	268.92	18.22	2.12
	2			232.58	16.02	
CP-60-2-12.5	1	2.0	71.30	278.76	18.73	2.25
	2			281.92	19.26	

Figure 3 – Load-slip curves of the direct shear tests on prismatic specimens
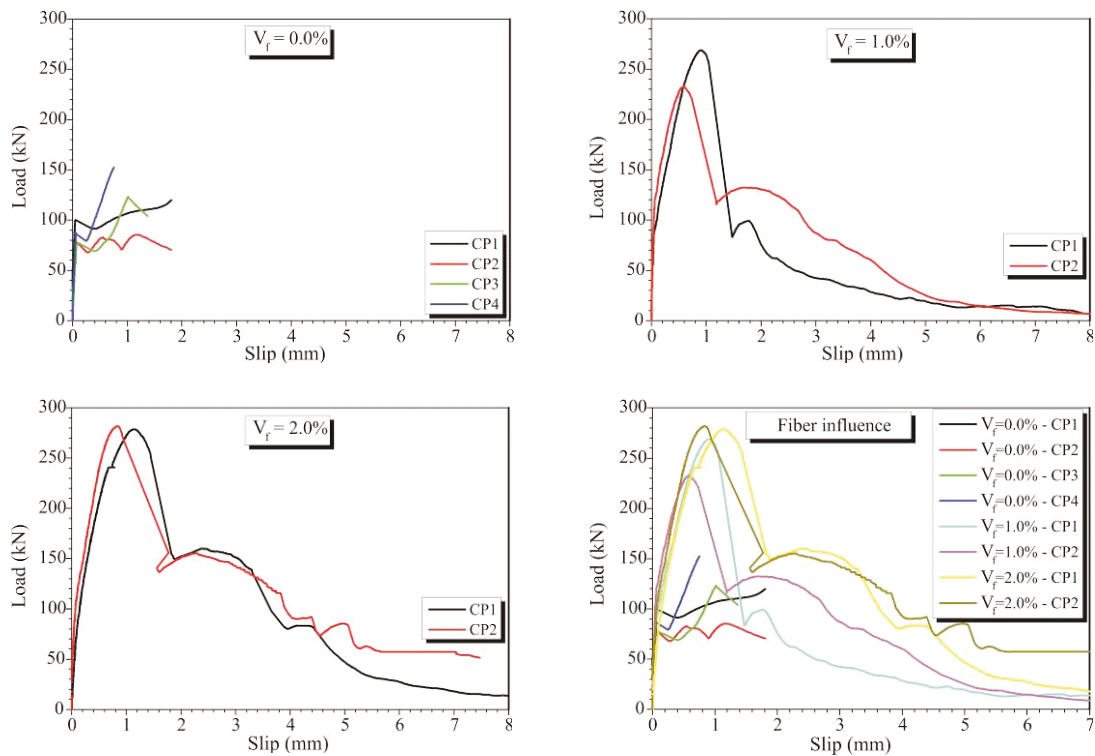
The influence of the fibers can also be noted from the test results. In the specimens without fibers, it is not observed a softening curve after the shear strength is reached. The addition of fibers increases sensibly the shear strength. Moreover, when the peak load was reached, it is observed a notable softening response of the specimen due to the fibers. It is observed, also, the abrupt decrease around 60% in the shear strength after the peak load in the mixture with 1% fiber amount while in the mixture with 2% fiber amount, this abrupt decrease was around 50%.

From the curves shown in Figure 3, the energy dissipated for a specific slip value can be determined for each test. Computing the energy for different slip values in the shear plan allowed the design of the curves shown in figure 4. These curves represent the energy dissipated by the shear plan for each specific slip. The toughness of the material is greater as much as the more energy dissipated. This figure shows that a fixed slip value of 1.5 mm, the addition of 1.0% and 2.0% amount of fiber increased the energy in 106% and

Table 4 – Parameters of the stress-strain tensile curve obtained from the computational modeling (15)

Fiber Volume Amount - V_f	f_{cm}[a] (MPa)	$f_{ct,num}$ (MPa)	$\varepsilon_{1,num} = \dfrac{f_{ct,num}}{E_c}$ (‰)	$0{,}5f_{ct,num}$ (MPa)	$\varepsilon_{2,num}$ (‰)	$\varepsilon_{3,num}$ (‰)
0.0%	53.60	4.410	Linear tension softening			
1.0%	65.27	3.280	0.111	1.640	12.0	50.0
2.0%	51.67	4.810	0.123	2.405	11.0	100

[a] Average compressive strength obtained in the test.

Figure 4 – Energy vs. slip curve of the direct shear tests on prismatic specimens
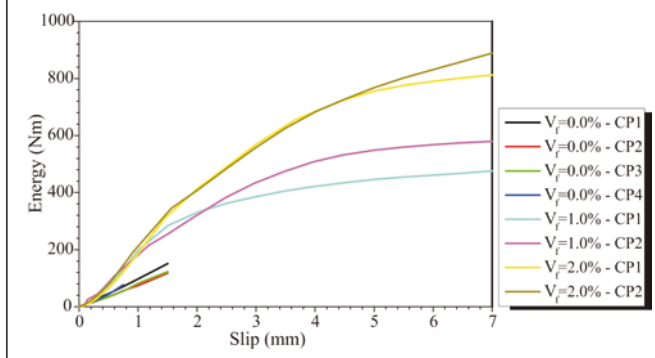
151%, respectively, when compared to the mixture without fibers. After this slip value, only the specimens with fibers could bear load. For the slip of 7 mm, the mixture with 2.0% fiber amount dissipated 61% more energy than the mixture with 1.0% fiber amount.

5. Computational modeling

5.1 Direct Shear tests

Firstly, the direct shear tests described in section 3.2 were modeled in the Finite Element Method software DIANA© 8.1.2 in order to determine the shear retention factor (β) for both the plain and the fiber reinforced concrete. For that reason, a bi-dimensional modeling was applied considering the Multi-Directional Crack Model with the smeared cracking included in the software [10]. It is worth mentioning that due to the defined fracture plan of the specimens, the discrete crack model could be adequate. Nevertheless, the smeared crack model was adopted due to the difficulty in modifying the mesh when the discrete crack model is applied to the modeling of structures without a defined fracture plan.

Figure 5 – Typical stress-strain tension relationship for fiber reinforced concrete
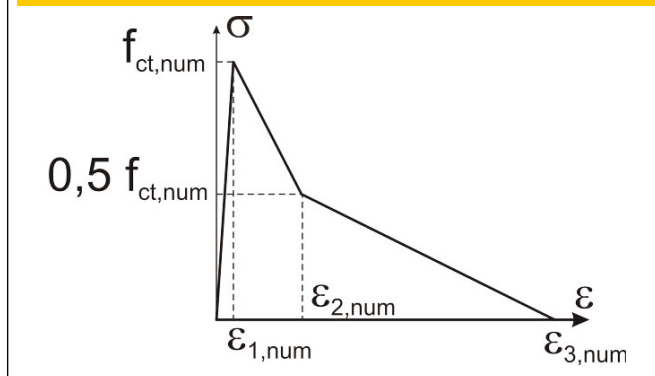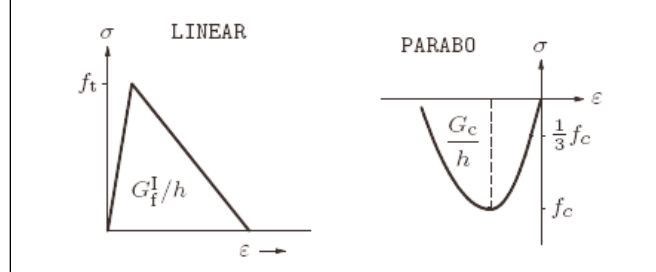

Figure 6 – Pre-defined tension softening and compression softening curves of concrete (9)

One of the most important parameters for the modeling is the tensile behavior of the concrete. It is difficult to determine a tensile behavior, including the tension softening, from the experimental tests; hence it was obtained here through the inverse analysis of the third-point bending tests in prismatic specimens using the DIANA© 8.1.2 software. The methodology used to obtain this curve had been previously described by the authors in other studies [15]. From the inverse analysis, the bilinear tension softening curve was defined, which proved more adequate to represent the fiber reinforced concrete used in this paper. Figure 5 shows a typical stress-strain curve. Table 4 shows the parameters of this curve for each fiber amount analyzed.
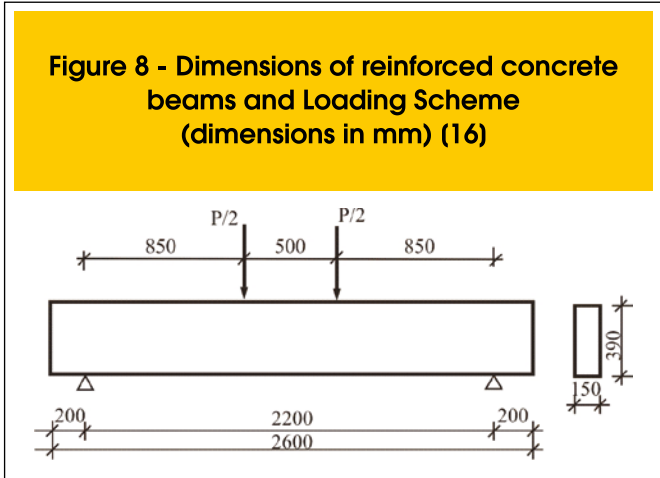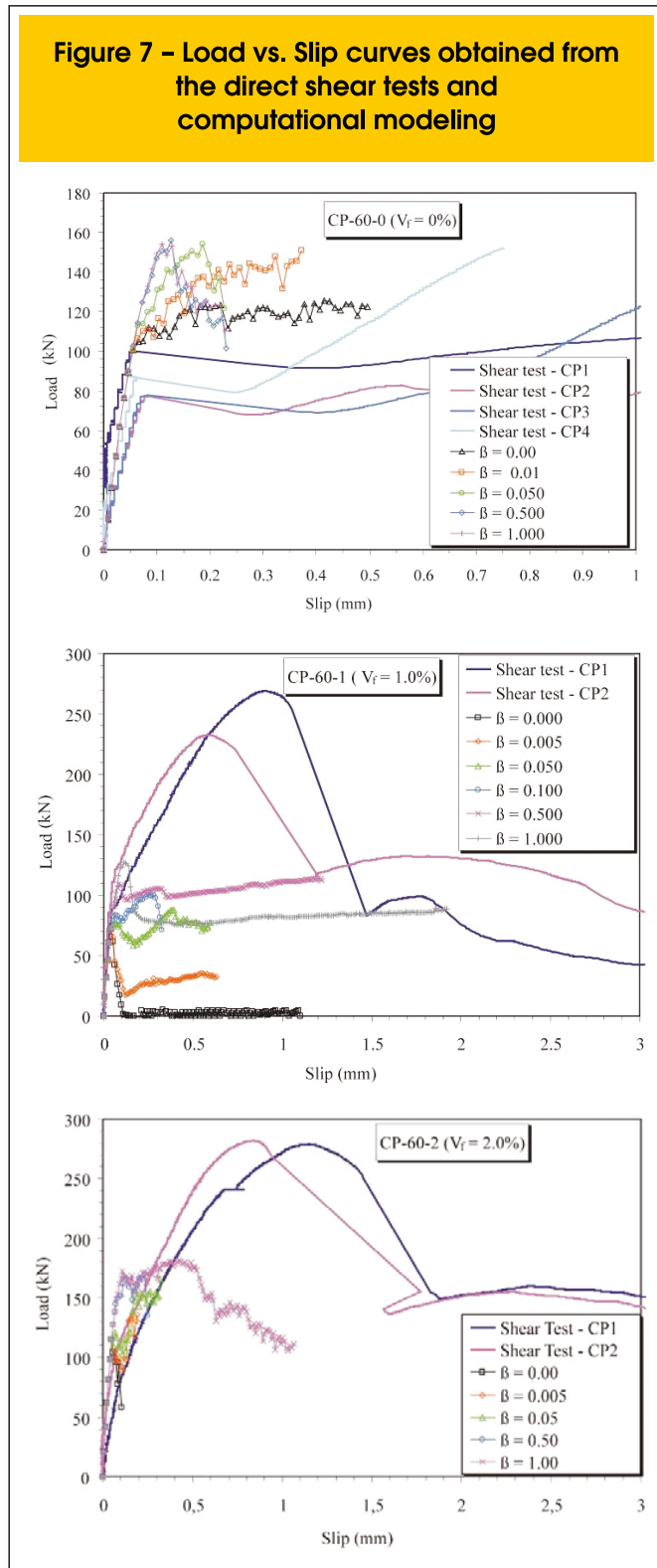
In order to represent the behavior of the concrete without fibers, a linear tension softening was used to represent the tensile behavior and a parabolic hardening/softening curve was used to represent the compression behavior, as shown in figure 6. The fracture energy (G_f^I) was obtained from the CEB-FIP Model Code 1990 [11] expressions. The compressive fracture energy (G_c) was obtained from the stress-strain relationship defined in CEB-FIP Model Code 1990 [10] to concrete in compression.

A study of the influence of the shear retention factor (β) on the direct shear response from the computational modeling was conducted. Accordingly, the following shear retention factor values were adopted 0; 0.005; 0.010; 0.050; 0.100; 0.150; 0.200; 0.500; and 1.000. For this analysis, the stress-slip curves of the direct shear tests were compared.

Figure 7 shows the experimental curves and those obtained from the computational modeling. For the specimens without fibers, it seems to be little influence of the shear retention factor since the maximum load varied within the range 100 kN to 160 kN when the β factor varied from 0 to 1. Such variation range is in accordance with that observed for the maximum load in the direct shear tests of the specimens without fibers. The shear retention value of 0.01 was chosen providing a force of 150 kN for the maximum slip of 0.4 mm.

The modeling results of the direct shear specimens with fibers do not represent the experimental curve completely. In addition, strong influence of the shear retention value on the softening response of the numerical model could be observed. A possible reason for that is due to the other resistant mechanisms that are present on the mode II of fracture concrete and which contribute more to the shear strength of those specimens. The most important of these mechanisms is the bridge effects provided by the fibers anchored at the

opposite sides of the shear crack that cannot be represented in a smeared crack model considering only the mode I of the fracture concrete. Hence, the shear retention factor of the fiber reinforced

Figure 7 – Load vs. Slip curves obtained from the direct shear tests and computational modeling

Figure 8 - Dimensions of reinforced concrete beams and Loading Scheme (dimensions in mm) (16)

concrete was reevaluated trough the computational modeling of reinforced concrete beams available in the literature.

5.2 Reinforced concrete beams

Once the direct shear specimens with and without fibers were ready, six reinforced concrete beams reported in the literature [16] were modeled. Figure 8 shows a scheme of those beams and the loading system used to promote a diagonal shear failure. Two beams were made of plain concrete and four beams were made of steel fiber reinforced concrete. One of the plain concrete beams did not have a transverse reinforcement (V-0-0.0) and the other had 0.21% of transverse reinforcement (V-1-0.21). The beams with fibers were reinforced with different amount of fibers (1% and 2%). Two beams with 1% fiber content were tested; one without transverse reinforcement (V-1-0.0) and the other with 0.21% of transverse reinforcement (V-1-0.21). Similarly, two beams with 2% fiber content were tested; one without transverse reinforcement (V-2-0.0) and the other with 0.21% of transverse reinforcement (V-2-0.21).

An eight-node isoparametric solid brick element (HX24L) was used for modeling the beams. This element is based on linear interpolation which enable that the nodal displacement vary linearly. The strain and stress distribution over the element volume are constant in one direction and vary linearly in normal directions. A *2x2x2* Gauss numerical integration schemes was adopted. This element has three degrees of freedom (translation) per node [10].

The embedded reinforcement element was used to represent the longitudinal and transverse reinforcements. This element is embedded inside the beam disregarding the slip between the reinforcement and the concrete. Thus, the compatibility of the nodes displacement is guaranteed resulting in a perfect bonding model between the reinforcement and the concrete.

The Total Strain model with fixed crack was used to represent the concrete. The tensile behavior of concrete without fibers was modeled using a linear tension softening, and a bilinear tension softening was used to represent the tensile behavior of the fiber reinforced concrete. For compression, a parabolic hardening/softening curve was used. The parameters in this model are: the tensile and compressive strength, the fracture energy (G_f^I), the compressive fracture energy (G_c) and the shear retention factor (β), which is constant during the increase in structure displacement.

Table 5 – Parameters to model the reinforced concrete beams

Beam	Fiber Volume Amount - V_f	f_{cm} [a] (MPa)	$f_{ct,num}$ (MPa)	$\varepsilon_{1,num} = \dfrac{f_{ct,num}}{E_c}$ (‰)	$0.5f_{ct,num}$ (MPa)	$\varepsilon_{2,num}$ (‰)	$\varepsilon_{3,num}$ (‰)
V-0-0.0	0.0%	46.30	3.92	Linear tension softening (G_f = 0,121 N.mm/mm^2)			
V-0-0.21	0.0%	47.23	3.36	Linear tension softening (G_f = 0,121 N.mm/mm^2)			
V-1-0.0	1.0%	56.87	3.28	0.103	1.640	12.0	50.0
V-1-0.21	1.0%	52.89	3.28	0.112	1.640	12.0	50.0
V-2-0v0	2.0%	51.67	4.81	0.123	2.405	11.0	100.0
V-2-0.21	2.0%	62.00	4.81	0.144	2.405	11.0	100.0

[a] Average compressive strength obtained in the test.

The compressive fracture energy was obtained from the stress-strain relationship defined in CEB-FIP Model Code 1990 [11] to concrete in compression. For the fiber reinforced concrete beams, the complete stress-strain curve in tension is provided instead of the fracture energy. The input parameters for the modeling of the six reinforced concrete beams are shown in table 5.

Figure 9 shows the curves obtained from the computational modeling of the reinforced concrete beams. It also shows the curves obtained experimentally. It can be noted that the shear retention factor (β) influenced the response of the beams without fibers. There was an increase in the stiffness and ultimate load of the beam with the increase in the value of the factor β. The best approximation between the numerical and experimental curves occurred for the β value of 0.01 confirming the analysis performed for the direct shear specimens. It is worth mentioning that the highest difference was found between the curves of beams without fibers and stirrups (V-0-0), in which there was a one single diagonal crack linking the support to the loading point without a major beam cracking (figure 10).

Analyzing the fiber reinforced beams, it can be noted that there was little influence of the shear retention factor (β) on both the beams with and without stirrups. Therefore, it can be said that the significant increase of the ultimate strain on the tension softening diagram caused by the fibers minimized the influence of the shear retention factor on the structure response. In that case, the best approximation between the numerical and experimental curves occurred for the β value of 0.15. It is noteworthy to mention that the highest difference observed between the curves of beams with 2% fiber amount and no stirrups (V-2-0) is due to problems found in the tests with this beam, as mentioned in the literature [16].

Figure 11 shows the strain of the longitudinal reinforcement in the middle of the span obtained from the modeling. This figure also shows the strain obtained experimentally. Again, it can be observed a stronger influence of the shear retention factor on the beams without fibers and lesser influence on the fiber reinforced beams. In this case, however, it can be seen that the stiffness of the numerical response was greater than that observed in the experimental curves for all beams. This is probably due to the sup-posed perfect bonding between the longitudinal reinforcement and the concrete, which tends to stiffen the structure due to disregard the slip between the reinforcement and the concrete.

Figure 12 shows the strain of the stirrup that intercepts the larger opening diagonal crack obtained from the modeling. This figure also shows the strain obtained experimentally. It could be observed that the numerical response was stiffer than the experimental response. This is due to the fact that there were principal diagonal cracks in all tested beams concentrating stress in the stirrup, a fact that could not be represented using the smeared crack model. Even though, the smeared crack model was adopted since it is difficult to predict the crack path in a discrete crack model.

Table 6 shows the ultimate shear strength in beams obtained experimentally and those of the computational modeling. Shear retention factor values of 0.01 and 0.15 were used for concrete without and with fibers, respectively. It is worth mentioning that the ultimate shear strength of the beam V-0-0 shown in this table is higher than that shown in figure 9. This occurred because the displacement transducers that measured the displacements were withdrawn before the end of the test [16]. The average value of the ratio between the numerical and the experimental shear strength was 1.021 with a standard deviation of 0.092. This indicates that the computational modeling of this study represented the failure of the beams accurately.

The crack tip openings were then determined by the computational modeling and the values were compared to those obtained experimentally. Table 7 shows those values in millimeters. The values in parentheses indicate the load, in kN, at the moment the crack was determined for both the test and the computational modeling. The cracks were evaluated for three levels of loadings, i.e., 40%, 60%, and 100% for the ultimate load on each beam, approximately. In this table, the crack tip openings were calculated using the diagonal distance between the finite element nodes chosen for the analysis. This choice was based on the finite element with the larger shear crack tip opening. The experimental value was obtained from the literature [16], and it is taken as close as possible to the finite element chosen for the analysis.

Generally, the numerically determined crack tip opening values shown in this table are closer to those measured in the tests for all levels of loadings; except for the V-0-0 beam, without fibers and stirrups, in which the numerically determined openings were rather lower than the experimental values. This is due to the failure pattern of this beam, which resulted in a single diagonal crack from the support to the loading point without developing a multiple cracks. Thus, the smeared crack model was found to be inadequate to evaluate the cracking pattern of a plain concrete beam without stirrups.

This methodology to evaluate crack tip openings was initially adopted by the authors who studied reinforced concrete beams, without fibers but with stirrups, subjected to shear, and it provided good approximation to the experimental values [17]. Although simple, this methodology is useful for three dimensional structures. In his kind of structure, such as spillway columns and hydroelectric plant spiral casings, the simplifications presents on the majority standards for the evaluation of the reinforced concrete crack tip openings can not be applied.

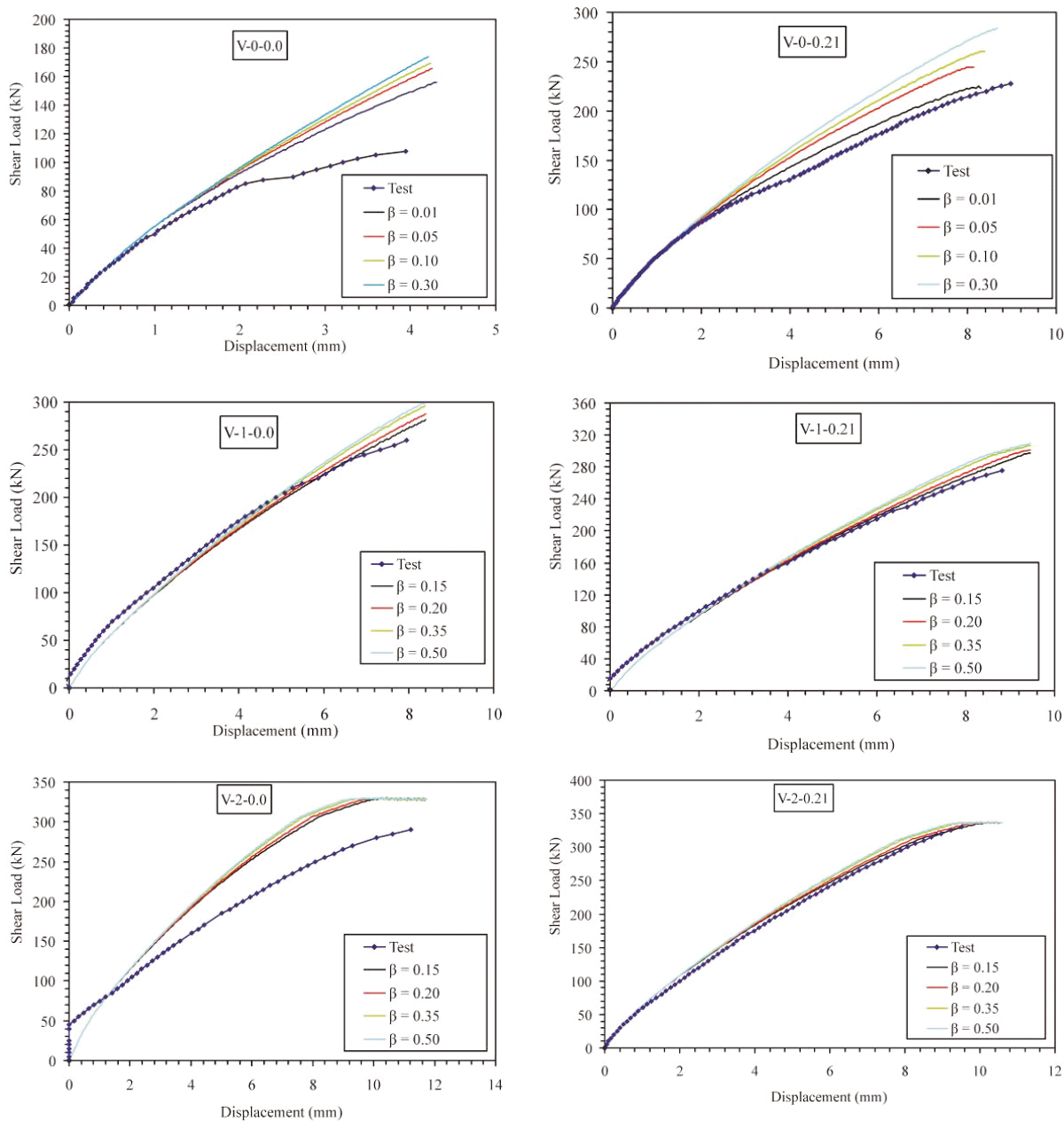**Figure 9 – Load vs. displacement in the middle of the span of reinforced concrete beams**

Table 6 – Ultimate shear strength of reinforced concrete beams

Beam	$V_{u,exp}$ [a] (kN)	$V_{u,num}$ [b] (kN)	$V_{u,num}/V_{u,exp}$
V-0-0.0	172.5	156.0	0.90
V-0-0.21	228.5	225.0	0.98
V-1-0.0	260.0	281.5	1.08
V-1-0.21	275.5	297.6	1.08
V-2-0.0	290.5	329.6	1.13
V-2-0.21	360.0	337.2	0.94

[a] $V_{u,exp}$: ultimate shear strength obtained experimentally;
[b] $V_{u,num}$: ultimate shear strength obtained from the modeling.

Figure 13 shows the cracking patterns of the beams reinforced with stirrups close to the failure obtained from the computational modeling. The red lines indicate the greater opening cracks. It can be seen that the failure of the beams without fibers and the ones with 1% fiber amount (V-0-0.21 e V-1-0.21) were due to shear, as observed in the tests, whereas the 2% fiber amount beam (V-2-0.21) presented shear and bending cracks in the middle of the span, confirming the experimental observation once this beam failure is due to bending and not to shear.

6. Conclusions

This paper approached computational modeling of fiber reinforced concrete beams subjected to shear using the Finite Element Method software DIANA© 8.1.2. The following conclusions can be drawn:

■ The direct shear tests indicated that the steel fibers are effective in increasing the shear strength of concrete. Adding 1% fiber amount increased the ultimate shear strength of the concrete in 87% while adding 2% fiber amount increased it in 99%. Moreover, the fibers provided a stable softening behavior after peak load to the specimens enabling more energy dissipation.

■ The modeling of the direct shear tests indicated an adequate shear retention factor value of 0.01 (β) for the concrete without fiber. This value was confirmed by the modeling of re

Table 7 – Crack tip openings in reinforced concrete beams evaluated by the nodal coordinates of the finite element (in millimeters)

Beam	F1 = 40% Exp.	F1 = 40% Num.	F2 = 60% Exp.	F2 = 60% Num.	F3 = 100% Exp.	F3 = 100% Num.
V-0-0.0	0.00 (70)	0.000 (69)	1.00 (100)	0.011 (102)	2.40 (170)	0.189 (170)
V-0-0.21	0.03 (100)	0.007 (106)	0.20 (160)	0.128 (157)	0.53 (230)	0.715 (262)
V-1-0.0	0.05 (110)	0.028 (114)	0.10 (170)	0.164 (170)	0.73 (260)	0.486 (283)
V-1-0.21	0.00 (120)	0.037 (121)	0.20 (180)	0.195 (181)	0.60 (280)	0.525 (299)
V-2-0.0	0.02 (130)	0.007 (134)	0.10 (190)	0.096 (194)	0.45 (290)	0.451 (328)
V-2-0.21	0.02 (130)	0.002 (134)	0.10 (200)	0.111 (201)	0.30 (360)	0.491 (337)

Figure 10 – Failure of the beams tested (16)

(a) V-0-0

(b) V-0-0,21

inforced concrete beams. On the other hand, the shear stress-slip curve obtained from the tests to specimens with fibers could not be represented by the computational modeling once the resistant mechanism provided by the fibers throughout the shear cracks was not represented in the modeling.

■ The modeling of the reinforced concrete beams without fibers indicated the influence of the shear retention factor (β) on the beam strength. Generally, a value of 0.01 for this factor

is suggested since there is a small contribution of the crack shear strength on the shear strength of the structure.

■ The modeling of the reinforced concrete beams with steel fibers indicated a small influence of the shear retention factor (β) on the beam strength. In general, a value of 0.15 for this factor is suggested. With this value, it was observed a good correlation between the numerical and experimental ultimate load of the beams. The ratio between these loads was 1.021 with a standard deviation of 0.092.

Figure 11 – Load vs. longitudinal reinforcement strain in the middle of the span of reinforced concrete beams
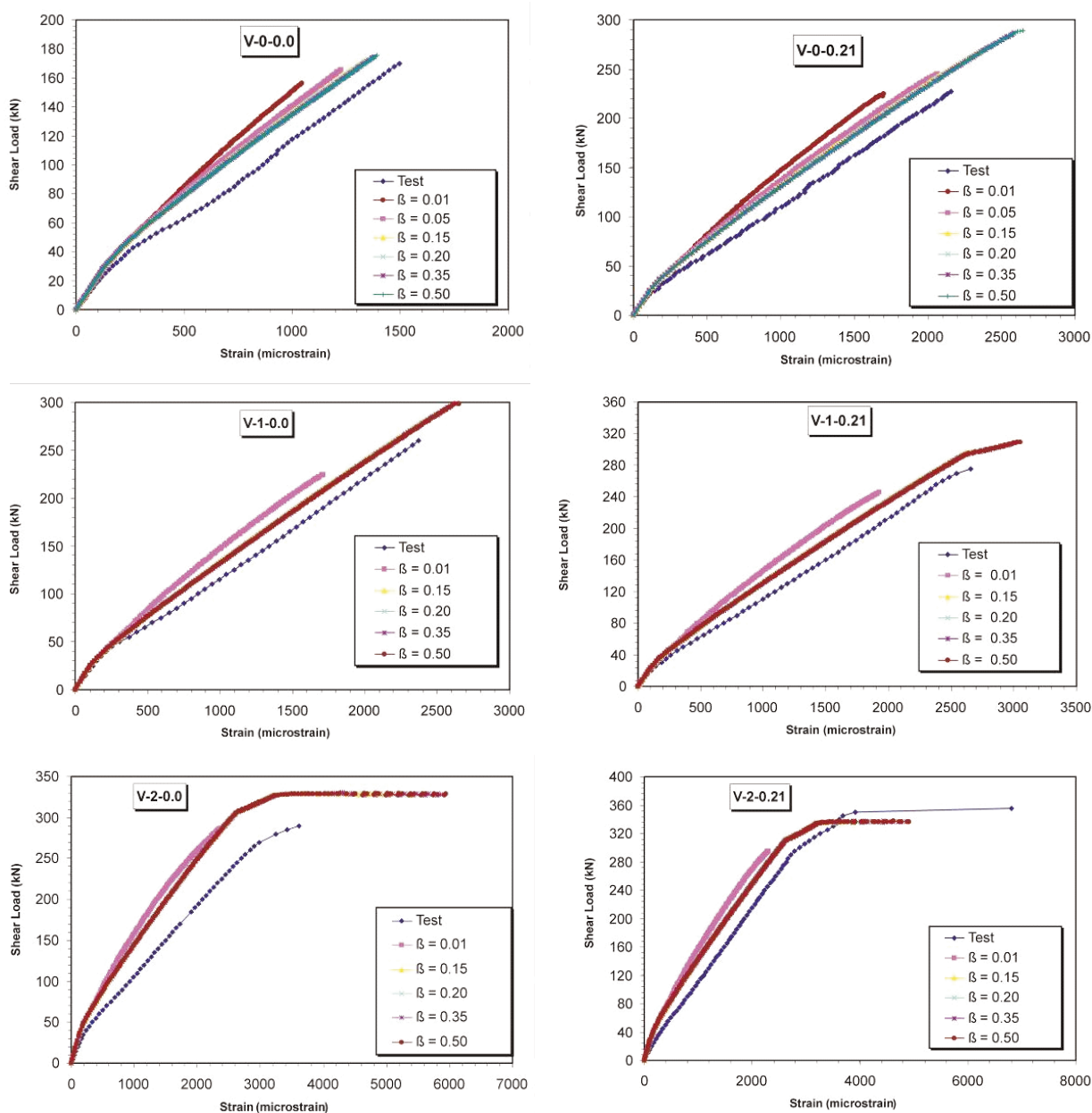
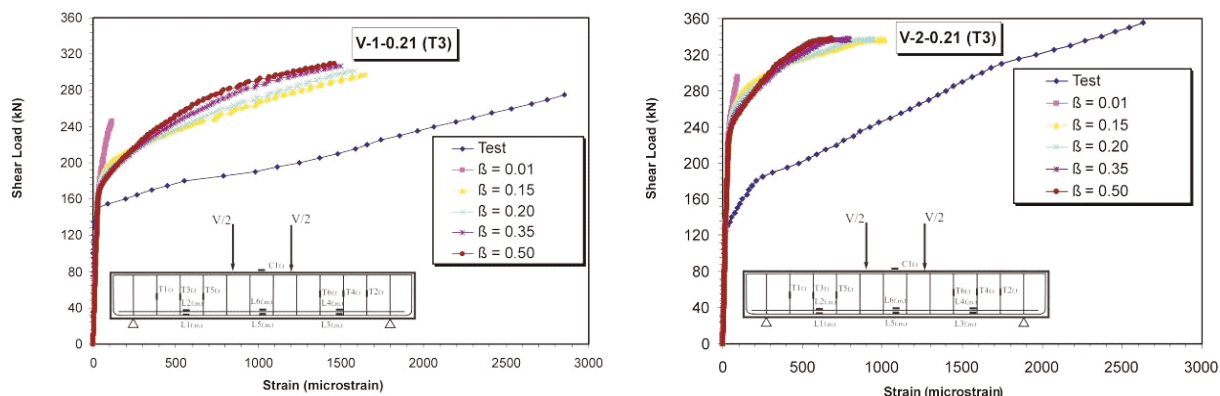Figure 12 – Load vs. stirrup strain of reinforced concrete beams
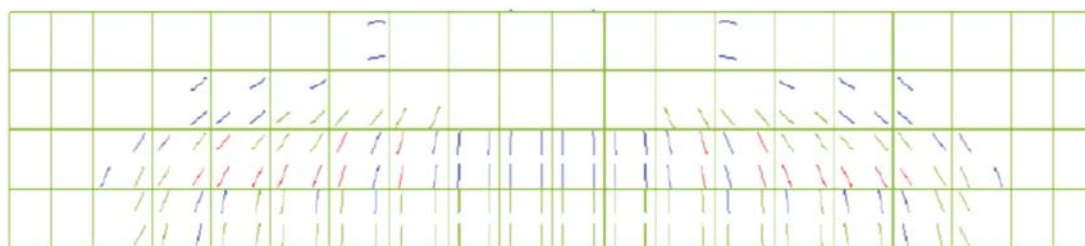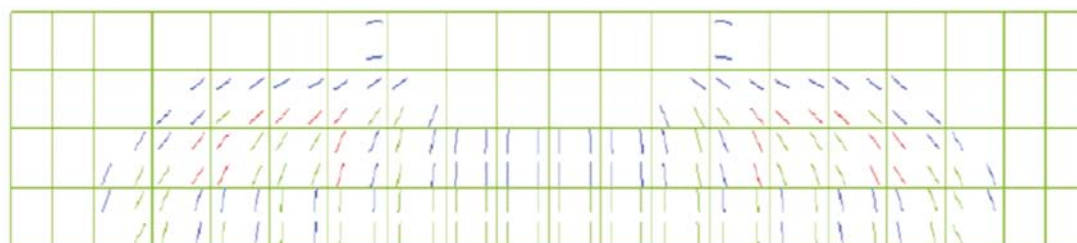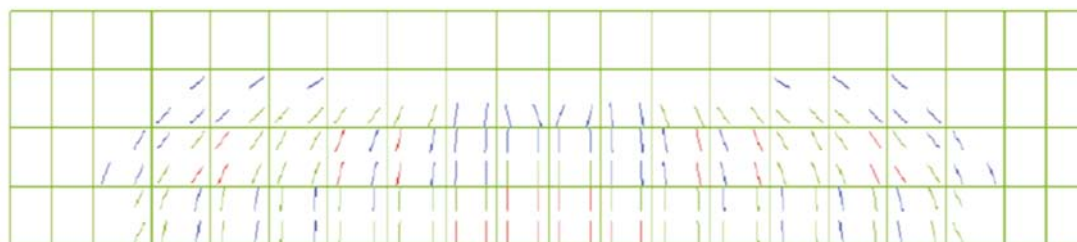

Figure 13 – Cracking patterns of reinforced concrete beams

(a) Beam V-0-0.21 – Load = 262.44 kN

(b) Beam V-1-0.21 – Load = 298.66 kN

(c) Beam V-2-0.21 – Load = 336.56 kN

■ The longitudinal reinforcement strain of the beams was adequately represented by the computational modeling despite the greater stiffness due to the supposed perfect bonding between the reinforcement and the concrete. On the other hand, the strain of the stirrups obtained from the modeling was smaller than that of the tests due to the failure pattern, i.e., there was a principal diagonal crack. This kind of failure could not be represented using a smeared crack model.

■ The modeling of the concrete beams also indicated a considerable reduction in the crack tip openings with the addition of steel fibers.

■ The methodology proposed to evaluate the crack tip openings, based on the smeared crack model, was found adequate to represent the crack tip openings observed on the tests. This is particularly interesting due to the fact that lack of a standard expression for determining shear crack tip openings, unlike what occurs for bending cracks. Therefore, this modeling methodology can be useful in the design of structures, mainly those in which the shear stress are preponderant as well as those that do not present one-dimensional behavior such as dams.

7   Acknowledgements

8   References

[01]   Vecchio, F.J.; Collins, M.P. The modified compression field theory for reinforced concrete elements subjected to shear. ACI Journal, n. 83, 1986, p.219-231.

[02]   Pang, X. B.; Hsu, T. T. C. Behavior of reinforced concrete membrane elements in shear. Structural Journal of the American Concrete Institute, v.92, n.6, 1995, p.665-679.

[03]   Hsu, T.T.C. Unified approach to shear analysis and design. Cement and concrete Research, n. 20, 1998, p.419-435.

[04]   Carmo, L.C. Ductilidade de vigas de concreto armado convencional e de alta resistência reforçadas com fibras metálicas: Análise via Método dos Elementos Finitos. 2005. 188 f. Dissertação (Mestrado em Engenharia Civil) – Escola de Engenharia Civil, Universidade Federal de Goiás, Goiânia.

[05]   Gálvez J. C.; Cervenka J.; Cendón D. A.; Saouma V. A discrete crack approach to normal/shear cracking of concrete strategy for problems in elasticity, plasticity, linear and nonlinear fracture mechanics. Technical Report, Department of Civil Engineering, University of Colorado, Boulder, and Electric Power Research Institute, Palo Alto, CA, 2002.

[06]   Hillerborg, A.; Modéer, M.; Petersson, P. Analysis of crack formation and crack growth in concrete by means of fracture mechanics and finite elements. Cement and concrete Research, n. 6, 1976, p.773–782.

[07]   Reich, R., Cervenka, J., and Saouma, V.. Merlin: A three-dimensional finite element program based on a mixed-iterative solution strategy for problems in elasticity, plasticity, and linear and nonlinear fracture mechanics.' Technical report, Electric Power Research Institute, Palo Alto, California, 1997.

[08]   Cervenka, V. Inelastic finite element analysis of reinforced concrete panels under in-plane loads. PhD thesis, University of Colorado, USA, 1970.

[09]   Souza, R. A. Concreto estrutural: Análise e dimensionamento de elementos com descontinuidades. 2004. 442f. Tese (Doutorado em Engenharia) – Escola Politécnica, Universidade de São Paulo, São Paulo.

[10]   TNO Building and Construction Research. DIANA User's Manual – Release 8.1. Delft, Netherlands, 2001.

[11]   COMITÉ EURO-INTERNATIONAL DU BÉTON. CEB-FIP Model Code 1990. London: Thomas Telford Services Ltd, 1993.

[12]   ASSOCIAÇÃO BRASILEIRA DE NORMAS TÉCNICAS. Concreto – Ensaio de compressão de corpos-de-prova cilíndricos. NBR 5739. Rio de Janeiro, 1994.

[13]   ASSOCIAÇÃO BRASILEIRA DE NORMAS TÉCNICAS. Argamassa e concreto – Determinação da resistência à tração por compressão diametral de corpos-de-prova cilíndricos. NBR 7222. Rio de Janeiro, 1994.

[14]   Mirsayah, A.A.; Banthia, N. Shear strength of steel fiber-reinforced concrete. ACI Materials Journal, v. 99, n. 5, 2002, p. 473-479.

[15]   Araújo, D.L.; Carmo, L.C.; Prado, A.A. Determinação da curva tensão-deformação à tração de concretos reforçados com fibras de aço via modelagem computacional. *In*: CMNE 2007 Congresso de Métodos Numéricos em Engenharia / XXVIII CILAMCE Congresso Ibero Latino-Americano sobre Métodos Computacionais em Engenharia, 2007, Porto. Métodos Numéricos e Computacionais em Engenharia - CMNE/CILAMCE. Porto, 2007. p. 1-16.

[16]   Nunes, F. G. T. Análise experimental de vigas de concreto reforçado com fibras de aço submetidas a esforços de cisalhamento. 2006. Dissertação (Mestrado em Engenharia Civil) – Escola de Engenharia Civil, Universidade Federal de Goiás, Goiânia.

[17]   Carmo, L.C.; Vanalli, L.; Araújo, D.L. Modelagem numérica de vigas de concreto armado submetidas a cisalhamento. *In*: XXVII CILAMCE - Iberian Latin American Congress on Computational Methods in Engineering, 2006, Belém. Proceedings, 2006. p. 1-14.